Available online at www.sciencedirect.com
SCIENCE DIRECT®
Journal of Power Sources 143 (2005) 275–283
JOURNAL OF POWER SOURCES
www.elsevier.com/locate/jpowsour

42 V Power Net with supercapacitor and battery for automotive applications

J.N. Marie-Francoise, H. Gualous *, R. Outbib, A. Berthon

L2ES, Université de Franche-Comté, UTBM, Rue Thierry MIEG, F90010 Belfort, France

Received 13 April 2004; received in revised form 6 December 2004; accepted 13 December 2004
Available online 17 February 2005

Abstract

This paper presents simulation and experimental realization of 42 V Power Net for automotive auxiliary on-board applications. For energy storage, a pack of supercapacitors is used in parallel with a battery. For simulation, the mathematical models of battery, DC/DC converters and supercapacitors are developed using MATLAB/SIMULINK®. An experimental power test bench has been designed. The 42 V Power Net voltage and the load current of supercapacitors are controlled by a microcontroller. Simulation results and experimental ones are presented, compared and analysed.

Keywords: Supercapacitors modeling; DC/DC converter; Energy sources control; Energy management

1. Introduction

Increase power consumption on automotive are making DC 14 V electrical systems inadequate. The total power demand will triple in some cars from 800 W today to average of 2500 W and to several kW range for peak demands in the future. This is because of some new equipment such as electromechanical valve, active suspension and drive-by-wire technology. The power requirements can be more efficient using higher voltage: 42 V DC voltage bus is one solution for this problem. Because of the increasing of peak power demand in modern power electronic applications, aluminium electrolytic capacitors can be used. These capacitors are able to supply a high current but for a few milliseconds. Another solution consists in using batteries; they are able to supply high currents for long time. Moreover, the cyclic behaviour of batteries is poor in comparison to capacitors and they present a low power density. Supercapacitor is a new device for energy storage. Its power density is considerably higher than that of batteries, and the energy density is higher than that of electrolytic capacitors. Moreover, it can be cycled several hundred thousand times. So, supercapacitor is ideally placed for peak power demand in transportation, for example [1–4].

Supercapacitors can be used in numerous applications, in electric or hybrid vehicles in order to provide peak power for improved acceleration, for energy recovery. In parallel with the vehicle battery during start up of an internal combustion engine with the purpose of decreasing the size and the power of the battery. In fuel cell vehicles, in order to reduce the power and therefore the cost of the fuel cell [5–7].

In this paper, we purpose to use supercapacitor in parallel with battery in 42 V hybrid power source for automotive applications, for peak power requirement. This is in order to increase the efficiency and the life cycle of the system, and to reduce the size of battery. First, we introduce supercapacitor structure and its model, after that we describe the operating system. Second, realization and test bench of the 42 V hybrid power source are presented, and finally simulation and experimental results are analysed and compared.

* Corresponding author. Tel.: +33 3 84 58 36 16.
E-mail address: hamid.gualous@univ-fcomte.fr (H. Gualous).

0378-7753/$ – see front matter © 2005 Elsevier B.V. All rights reserved.
doi:10.1016/j.jpowsour.2004.12.011

2. Supercapacitor description and modeling

2.1. Supercapacitor description

Supercapacitor is based on the double layer capacitor. The elementary structure consists of two activated carbon electrodes, which are immersed into electrolyte, and a separator that prevents physical contact of the electrodes but allows ion transfer between them [8–12]. Energy is stored in the double layer capacitor as a charge separation in the double layer formed at the interface between the solid electrode material surface and the liquid electrolyte in the micropores of the electrodes. The high energy content of supercapacitors in comparison to the electrolytic capacitors is due to the activated carbon electrode material, which has an extremely high specific surface area and the extremely short distance at the interface between electrode and electrolyte less than 1 μm. Thus, it is possible to obtain a very high capacitance, up to a few thousand Farads [9,13,14].

The supercapacitor capacitance is given by:

$$\frac{1}{1/C_{\mathrm{dl}}(1) + 1/C_{\mathrm{dl}}(2)}, \tag{1}$$

where $C_{\mathrm{dl}}(1)$ and $C_{\mathrm{dl}}(2)$ are the electric double layer capacitance at the two electrodes.

Supercapacitor functioning is based on an electrostatic effect, which is purely physical reversible [4,9]. This mode of energy storage is different of the battery, which is based on the formation and dissolution of chemical compounds at electrodes (faradic reaction). This difference allows a very high life cycle compared to the battery. Moreover, the performance characteristics of supercapacitor depend on the properties of the electrolyte. Two solutions are proposed. The first one is aqueous electrolyte. It limits the unit cell supercapacitor voltage typically 1.5 V, thus reducing the available energy significantly. Advantages of the aqueous electrolyte are higher conductivity (0.8 S cm^{-1} for H_2SO_4) and low cost. The second solution uses organic electrolyte, which has the advantage of a higher achievable voltage, typically 2.5 V. The cell voltage is most probably limited by the water content in the electrolyte. The organic electrolyte has a significantly higher specific resistance (the conductivity is typically 0.05 S cm^{-1}). This last also affects the equivalent distributed resistance of the porous layer and consequently reduces the maximum usable power, which depends on the total effective series resistance (ESR) of the supercapacitor. However, part of the reduction in power is compensated by the higher cell voltage achievable with an organic electrolyte. In our study, we have studied and used supercapacitors, which use activated carbon electrodes and organic electrolyte [15,16].

2.2. Supercapacitor modeling

To use supercapacitor in transportation applications, it is necessary to simulate the system in order to dimension its components and to optimize it. Furthermore, a model to describe the supercapacitor behaviour must be established. Two solutions are proposed in the literature. The first out proposes an equivalent circuit based on transmission-line model, which involves distributed capacitance C_i and resistance R_i [17,18]. R_i and C_i can be considered, respectively, as resistance and capacitance of the pores. The second solution proposes to describe the supercapacitor behaviour by an equivalent electric circuit with two RC branches [19]. This solution is not complex and the simulation time is reduced compared with the model of transmission line. In our study, we have used the model with two branches.

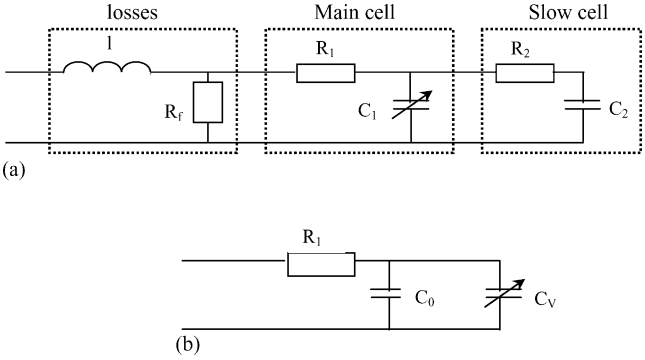

Fig. 1. Equivalent circuit of supercapacitor: (a) two branches model; (b) simplified model.

Fig. 1a shows the electric equivalent circuit of supercapacitor. Zubieta and Bonert [19–21] have showed that to define the structure of the equivalent circuit, three major aspects of the physics of the double-layer capacitor should be taken into account [19,20]. First, based on the electrochemistry of the interface between two materials in different phases, the double-layer capacitance is modeled by a two parallel resistive capacitive branches with different time constants. Second, based on the theory of the interfacial tension in the double-layer, it can be expected that the capacitance of the device depends on the potential difference. In the practical range of the double-layer capacitor, Zubieta and Bonert [19,20] have obtained that the differential capacitance measured experimentally varies linearly with the capacitor voltage. Third, the double-layer capacitor shows certain self discharge. A series inductor may be added for pulse applications. This inductance is so small (nano Henrys), it can be neglected in most applications in power electronics.

To reflect the voltage dependence of the capacitance, the first branch is modeled as a voltage dependent differential capacitor C_1. It consists of a constant capacitor C_o and a capacitor C_v whose value varies linearly with the voltage V_1 (i.e. $C_1 = C_o + kV_1$).

R_1 is the equivalent serial resistance. The R_1C_1 branch dominates the immediate behaviour of the supercapacitor in the time range of seconds. The R_1C_1 cell is the main branch, which determines energy evolution during charge and discharge cycles in power electronics applications (charge and discharge in a few seconds). It is called a fast branch. The R_2C_2 cell is the slow branch; it completes the first cell in long

time range in order of a few minutes and describes the internal energy distribution at the end of the charge (or discharge). R_f is the equivalent parallel resistance. The later has only impact on long-term storage performances since it is a leakage effect. R_f can be neglected during fast charge/discharge of the supercapacitor.

The parameters of the proposed model with two RC branches are identified carrying out a single fast current controlled charge. The parameters are identified by charging and discharging at constant current [19–21].

In the most of power electronic applications, supercapacitor is used to provide a peak power in transient state with a few seconds. For this reason, the slow branch R_2C_2 can be neglected. To valid this hypothesis, a Maxwell BCAP0010 of 2600 F is modelling only by the R_1C_1 circuit described previously, Fig. 1b shows the supercapacitor equivalent circuit used in this study when the time of charge and discharge cycle is less than 100 s.

The parameters of the proposed model can be identified carrying out a single fast current controlled charge. The experimental method to determine the parameters of the supercapacitor equivalent circuit is described in [19,21]. In our study, we have charged and discharged the 2600 F at constant current (108 A), the obtained values are:

- $R_1 = 0.64\,\text{m}\Omega$;
- $C_0 = 1862$ F;
- $k = 308\,\text{F V}^{-1}$. At the nominal voltage $V_1 = 2.5$ V; $C_v = kV_1 = 770$ F;
- The global capacitor is $C_1 = C_0 + C_v = 2632$ F.

These values are in good agreement with the Maxwell 2600 F specifications listed in Table 1. Using the supercapacitor model determined previously, Fig. 2 presents the experimental and simulation results of the 2600 F. The charge and discharge are realized at constant current, respectively, 96 and 50 A. It is clear that the simulation results with the fast R_1C_1 branch model and the experimental ones are similar.

Table 1
The specifications of the 2600 F supercapacitor

Specifications	
Capacitance (F)	2600 (DC, 25 °C)
Capacitance tolerance (%)	+20/−20
Voltage (V)	
Rated	2.5
Maximum	2.8
Serial resistance (mΩ)	0.7 (DC, 25 °C)
Specific power density (W kg^{-1})	4300 (2.5 V)
Current (maximum) (A)	600
Temperature (°C)	
Operating	−35 to 65
Storage	−35 to 65
Life time (25 °C) (years)	10
Cyclability (25 °C, $I = 20$ A)	500,000

The difference between the two results at the end of supercapacitor discharge is due to the fact that discharge current is not regulated by the active load used. This difference is obtained when the supercapacitor voltage is less than IV. Furthermore, it can be concluded that the model with one branch is verified by the present results and the hypothesis is valid.

The supercapacitors pack used is composed by eight supercapacitors of 2600 F in series. Using the same method described previously, we have determined the equivalent circuit of the pack composed by one branch R_1C_1. The experimental values of the model are:

- $R_1 = 5.2\,\text{m}\Omega$;
- $C_0 = 262$ F and $k = 3\,\text{F V}^{-1}$;
- At the nominal voltage $V_1 = 20$ V; $C_v = kV_1 = 60$ F;
- The global capacitor is $C_1 = C_0 + C_v = 322$ F.

These results are in good agreement with the values calculated from the constructor specifications (Table 1): the global capacitor is 2600 F/8 = 325 F and the total serial resistance

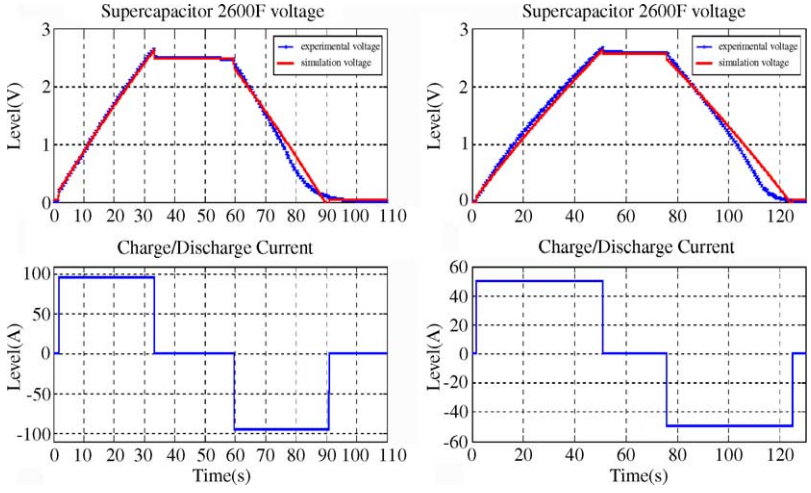

Fig. 2. Charge and discharge of BCAP0010 supercapacitor: simulation and experimental results.

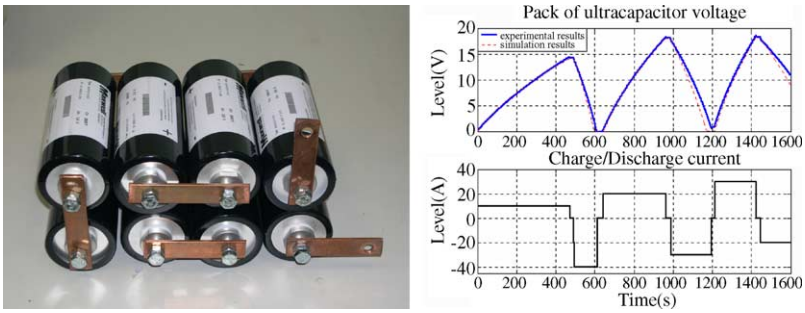

Fig. 3. Pack of eight supercapacitors in series and comparison between simulation and experimental results for different charge and discharge current.

is $8 \times 0.6\,\text{m}\Omega = 4.8\,\text{m}\Omega$. Fig. 3 shows the tests for which the simulations have been carried out using first charging and discharging the supercapacitors pack under constant current for different values. Simulation voltage curve is closed to the experimental one. These results obtained are satisfactory and will allow the validation of the model with the fast R_1C_1 branch described previously.

In conclusion, we have shown that the proposed model with one branch is validated for one supercapacitor and for a pack of supercapacitors. These, when the supercapacitors are used in power electronic applications, and when charge and discharge cycles are in order of 100 s.

3. Design and energy management of the system

3.1. Design of the system

Fig. 4 shows a diagram of the hybrid alimentation with supercapacitors pack and a lead acid battery for 42 V auto-

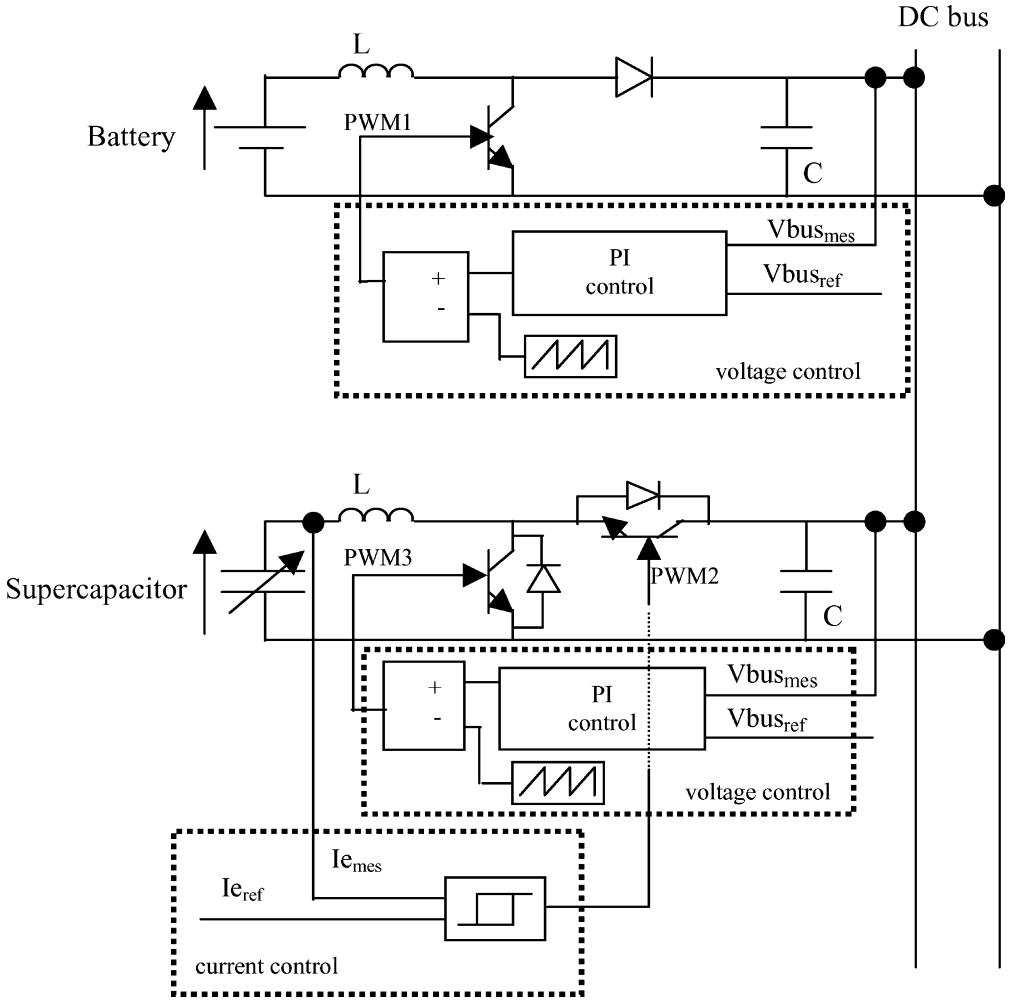

Fig. 4. 42 V Power Net for automotive electrical system applications.

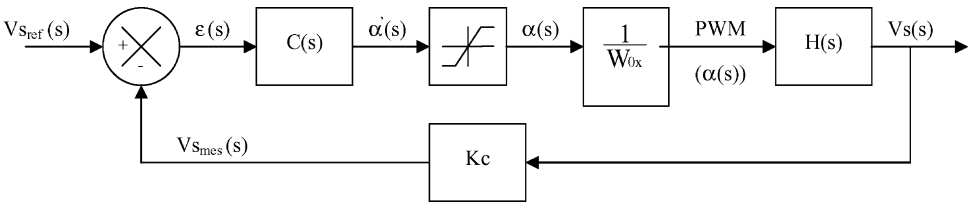

Fig. 5. Block diagram of the voltage control.

motive electrical system. The battery provides the required energy in steady state. The supercapacitors pack gives the required power of the automotive electrical system in transient state. The pack is sized to give approximately 2 kW during 10 s. It is composed by eight cells of 2600 F in series. During the power demand in the transient state by the automotive auxiliary, the supercapacitors pack provides the power requirement. The supercapacitors pack is discharged between the maximum voltage 18 V and the minimum of the discharge state 8 V, the battery is disconnected.

In steady state, the battery gives the power requirement for the supercapacitors pack charge and for automotive auxiliary alimentation for example. The DC bus voltage is controlled and regulated at 42 V.

The adaptation between the battery voltage level (12 V) and the DC bus voltage level (42 V) is realized by a boost DC/DC converter. It is composed by a power IGBT transistor, an inductor and a power diode. The DC/DC converter between the supercapacitors and the DC bus is bidirectional. It is composed by two power IGBT transistor, and an inductor. The bi-directional converter operates in two ways: boost operation, used in transient state where the supercapacitors pack is discharged in the 42 V DC bus. Buck operation is used to charge the supercapacitors pack from the DC bus.

3.2. System control and energy management

The buck converter between the DC bus and the supercapacitors is used to charge the supercapacitor pack at constant current. Its control system is based on a hysteretic control with constant frequency. The duty cycle is defined by the current reference and the output current. Thus, the PWM2 signal generated is used to IGBT drive the transistor. The on/off of the IGBT regulate the current of supercapacitors charge.

The two boost converters between supercapacitors pack and the DC bus and between battery and DC bus are driven by PWM3 and PWM1 signals (Fig. 4). The studied system is a first order one with a disturbance at its input. For its control, a PI regulator is used. The error signal, between the reference value and the measured value, is injected in the PI compensator and then transferred to the PWM generator regulator. The switches drive pulses are generated at a fixed frequency with a duty cycle defined by the error signal. The switches drive pulses are generated at a fixed frequency.

3.2.1. Analysis of the boost control loop

The block diagram of the boost control loop is shown in Fig. 5.

Where $V_{s_{ref}}$: reference voltage (42 V); $V_{s_{mes}}$: measured voltage; V_s: output voltage; $\varepsilon(s)$: voltage error; $\alpha(s)$: duty cycle at the output of the controller; PWM: command signal of the switch; W_{0x}: amplitude triangular signal; $C(s)$: transfer function of the voltage controller; $H(s)$: transfer function of the converter.

The operating principle of the voltage control is based on the comparison between the reference voltage (42 V) and the measured one. This error is applied to the controller. The output of the voltage controller is compared with a triangular signal in the aim to generate a PWM signal, which command the converter switches.

To determine the controller parameter we need to know the converter transfer function or it is time response. The boost converter topology consists of linear inductor, capacitor and non-linear switches. It can be identified by a transfer function, which is determined from the electrical equations of the converter, or by a black-box approach [22]. In the first case, it is very difficult to take into account the switch losses [23]. Hence, it is very complicated to establish the converter transfer function using the electrical equations. In the second case, the converter can be identified using it is time response.

In this study, the transfer function of the boost converter was determined using the step response. The experimental response is shown in Fig. 6. It is clear that the system is stable and its response can be identified by a first order transfer

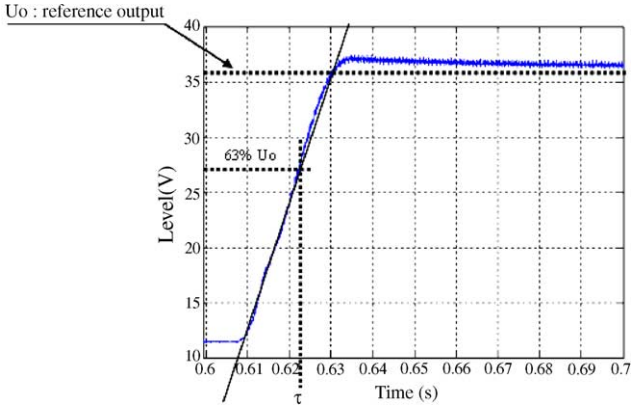

Fig. 6. Step response of the process.

function:

$$H(s) = \frac{K}{1+\tau s}$$

where K is the gain and τ is the time constant of the process.

From the experimental results, we have determined K and τ, respectively, 0.96 and 11 ms.

The most common controller structure in process applications is proportional-integral derivative (PID) controller [24,25].

- Proportional action decreases error in steady operation.
- Integral action returns the loop of precise regulation for instructions or disturbances constant.
- Derivative action makes the loop of regulation fast when the process has distant time-constants.

However, in our study the process is identified by a first order transfer function. Then, derivative action is thus useless. We, thus, chose a PI corrector [26,27].

The PI transfer function is:

$$C(s) = K_p\left[1+\frac{1}{T_i s}\right] = K_p + \frac{K_i}{s};$$

where K_p and T_i are, respectively, the gain and the time constant of the PI voltage controller and $K_i = K_p/T_i$.

Notice that saturation presented in Fig. 5 is used in the analysis as a security for the boost switch. Indeed when the control loop is failing, the duty cycle of the PWM signal is limited at 95%. However, and for some practices considerations this saturation can be omitted. Then, the saturation can be eliminated in the analysis. Therefore, the control loop can be simplified Fig. 7. A simple reasoning shows that the transfer function of the closed loop is:

$$G(s) = \frac{K_p K s + K K_i}{K K_i K_c + (1 + K K_p K_c)s + \tau s^2} \tag{2}$$

or, if s is replaced by $j\omega$

$$G(j\omega) = \frac{jK_p K\omega + K K_i}{K K_i K_c - \tau\omega^2 + j(1 + K K_p K_c)\omega} \tag{3}$$

Using Fig. 7, straight forward computations give the module and the argument of $T(j\omega)$ (transfer function of the open loop):

$$|T(j\omega)| = K K_c \frac{\left(\sqrt{(K_i\tau - K_p)^2\omega^2 + (K_i + K_p\tau\omega^2)^2}\right)}{\omega(1+\tau^2\omega^2)} \tag{4}$$

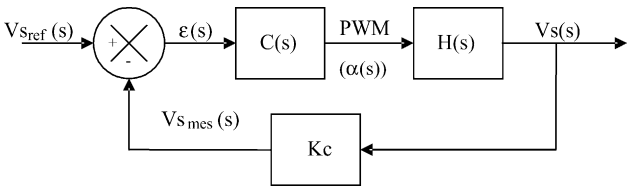

Fig. 7. Simplify block diagram of the voltage control.

and

$$\arg[T(j\omega)] = \text{arctg}\left(\frac{K_p\tau\omega^2 + K_i}{\omega(K_i\tau - K_p)}\right) \tag{5}$$

In our analysis, the PI controller parameters are assumed to satisfy the two following conditions:

- The margin of phase is at least equal to 90°.
- The poles must to be and in order to avoid oscillations, real negative.

Hence, using Eqs. (4) and (5), and in order to respect the conditions described before, the parameters must satisfied the following two equations:

$$K_i\tau - K_p < 0 \quad \text{or} \quad \frac{K_p}{K_i} > \tau \tag{6}$$

$$(1 + K K_i K_c) - 4K K_i K_c\tau > 0 \tag{7}$$

In practice, in order to have a robust control and to satisfy Eqs. (6) and (7); K_i is chosen to be higher than $100K_p$. Thus, in experimentation, we have fixed K_p and K_i to be, respectively, 0.7 and 75. Notice that the conditions described previously (see (6) and (7)) are respected. In order to illustrate the performances of the system, the Nichols's diagram for the closed-loop is given by Fig. 8. This result shows that the phase margin is in order of 90° and the margin gain is infinite. These are in good agreement with the predict results and the approximation of the system by a first order is seem to be correct.

3.2.2. Energy management

Power management of the system is realised by an algorithm procedure. The principle operation is as follows. In the algorithm, a threshold current is fixed in the steady state (I_{per}), the minimum and the maximum supercapacitors pack voltage levels are fixed, respectively, at $V_{sc_{min}}$ and $V_{sc_{max}}$. In the first, when the system is on, the pack of supercapacitors

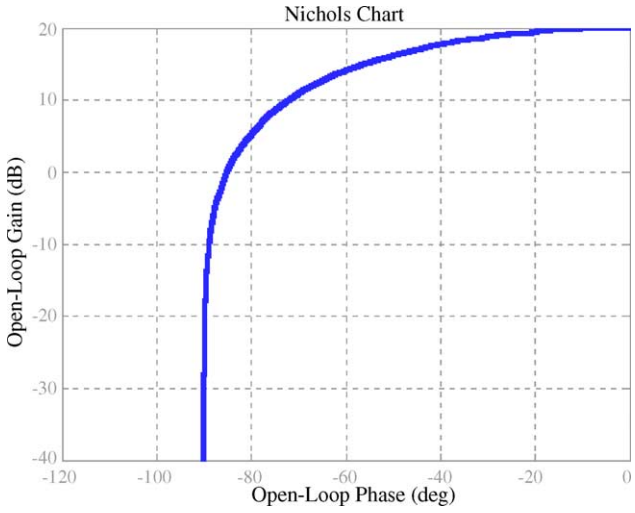

Fig. 8. Nichols diagram.

voltage V_{sc} is tested. If V_{sc} is less than $V_{sc_{max}}$, supercapacitors are charged until $V_{sc_{max}}$. After that, if the current demand at the DC bus is higher than I_{per} (transient state), battery is disconnected, the power requirement is given by the pack of supercapacitors. In the steady state, the battery provides the power requirement and the supercapacitors pack is charged.

If the current demand is higher than I_{per} and the $V_{sc} < V_{sc_{min}}$, the system can not provide the power requirements. Supercapacitors are charged from the battery.

4. Simulation results

The system, consisting of battery, supercapacitors, and DC/DC converters for automotive electrical system is simulated. The control and energy management, was developed using MATLAB/SIMULINK® software.

The battery is modelled by Shepherd equation [28]. The model of Shepherd is perhaps the best-known model of battery. Indeed, it describes the electrochemical behaviour of the battery directly in terms of voltage and current

$$E_t = E_o - R_i I - K_i \left(\frac{1}{1-f}\right) \quad (8)$$

where E_t: output voltage battery [V]; E_o: voltage of the battery with vacuum [V]; R_i: internal battery resistance [Ω]; K_i: polarization resistance [Ω]; I: instantaneous current [A]; f: battery accumulation of ampere-hour divided by the capacity integral.

The supercapacitors pack model used is described previously. DC/DC converters are modelized using mathematical equations, where the switches are supposed ideal (i.e. no losses). Initially, the converter, during boost mode operation, its voltage controlled using a PI corrector. For operation buck mode, a hysteresis control is used. Fig. 9 shows the hysteretic control and the two control loop for 42 V voltage regulation. In the steady state, the battery is connected and supercapacitors is charged, PWM2 and PWM1 are generated and PWM3 = 0, in the transient state, PWM1 = PWM2 = 0, PWM3 is generated.

The simulated electric vehicle (see Fig. 4) for illustration supply by a multi-source system is presented (Fig. 10).

Initially ($t = 0$), the pack of supercapacitors is charged to 8 V ($V_{sc_{min}}$). During the control of the process, the behaviour of the system is described as follows:

- $t \in [0;220]$: the supercapacitors voltage increases until 18 V ($V_{sc_{max}}$) with constant current (10 A). During the load

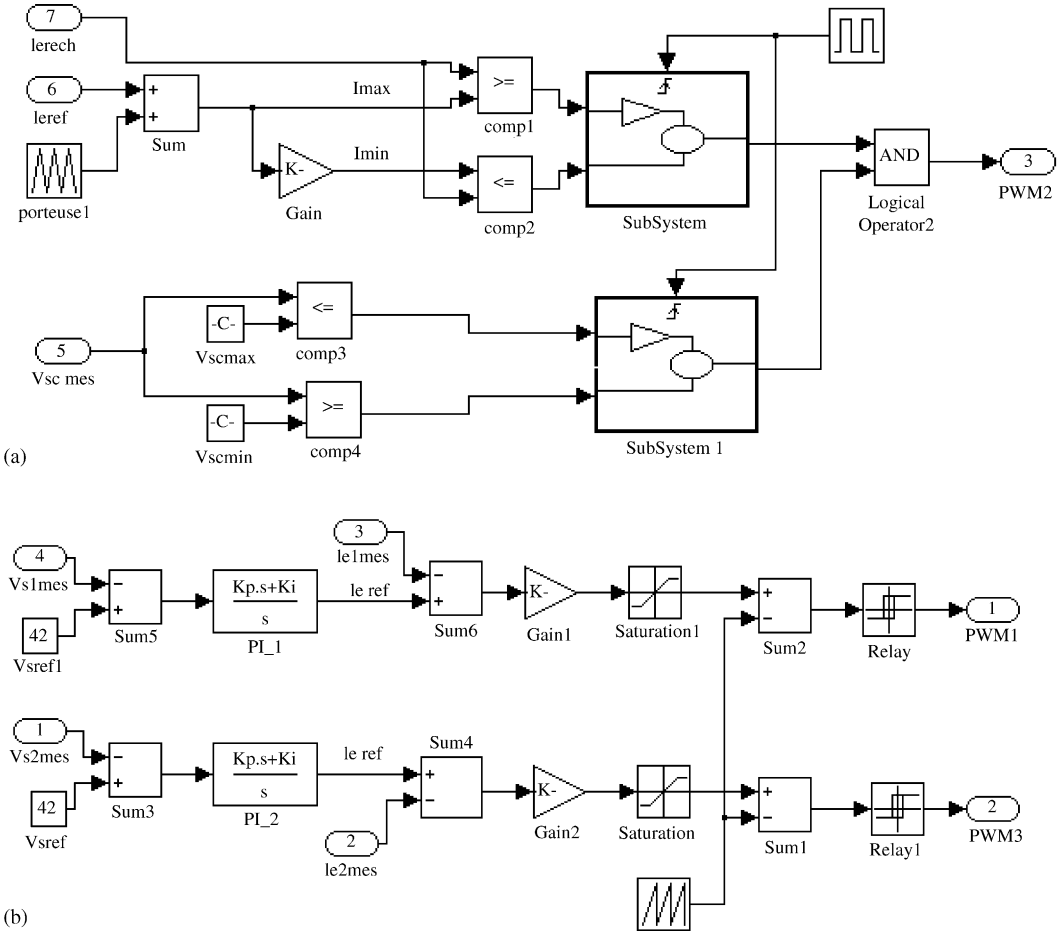

Fig. 9. Simulation of the system control (a) hysteretic control; (b) PI controller.

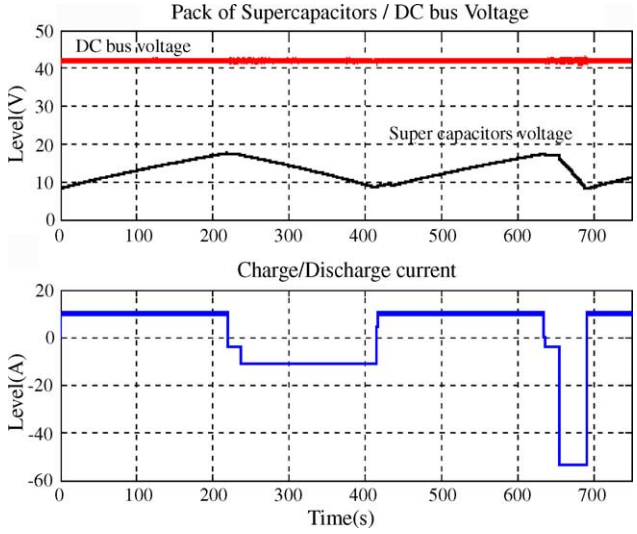

Fig. 10. Simulation results of the 42 V Power Net.

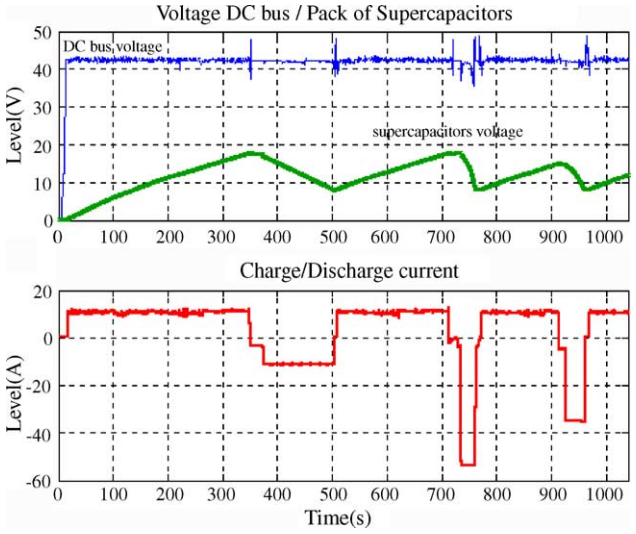

Fig. 11. Experimental results of the 42 V Power Net for automotive electrical system applications.

of the supercapacitors, the battery provides the 42 V on the DC bus.

- $t \in [220;415]$: the supercapacitors are discharged. During the current load variations, the battery stops providing energy, the supercapacitors discharge and stabilizes the voltage level on the 42 V DC bus.
- $t \in [417;635]$: once the supercapacitors are discharged, the charge cycle starts again.
- $t \in [638;691]$: supercapacitors are discharged at 54 A, battery is disconnected.
- $t \in [693;750]$: the pack of supercapacitors are charged from the DC bus.

Notice that, the DC bus voltage is maintained under constant value at 42 V whatever the load current variations on the DC bus. These results valid the control strategy and the power management algorithm.

5. Experimental results

An experimental test bench was developed to validate the model proposed in simulation using software MATLAB/SIMULINK®. The control and the power management of the system are realized by the Siemens SAB 167 microcontroller with CAN bus. Power switches are IGBTs, capacitor is 10 mF, and inductor is 60 μH. For the control and the power management, measurements are necessary: the supercapacitors current and voltage, the load current at the DC bus and its voltage. The measured voltage value at the DC/DC converters output is compared with a voltage reference, which is equal to the DC bus voltage (42 V). The generated error is corrected by a PI regulator in the two cases (when supercapacitors or battery provide the power requirement). The PI compensator and the hysteresis current regulation described previously are realized by the microcontroller. Currents and voltages are measured by LEM sensors and monitored by the microcontroller.

The experimental test of the 42 V Power Net for automotive electrical system is realized in the same configuration of the simulation conditions. Fig. 11 shows the evolution of the supercapacitors current and voltage and the DC bus voltage as a function of time.

During the control of the process, the behaviour of the system is described as follows:

- $t \in [17;350]$: supercapacitors are charging under constant current (10 A). The DC/DC converter between supercapacitors and DC bus operates in buck mode. The DC bus voltage is controlled at 42 V from the battery.
- $t \in [350;504]$: the supercapacitors are charged, then starts to discharge when the current on the DC bus varies. They discharge with various current values. The DC bus voltage remains constant to 42 V using supercapacitors energy and the DC/DC converter operates in boost mode.
- $t \in [510;730]$: the supercapacitors are discharged, they have to charge, the DC bus voltage is again controlled by the battery.
- $t \in [735;762]$: the supercapacitors are discharged by a high current.
- $t \in [774;914]$: the supercapacitors are not entirely charged but there is a current fluctuation on the DC bus, then, the supercapacitors are solicited in priority to maintain the DC bus voltage constant.

The experimental results show that the DC bus voltage remains constant to 42 V when the current load varies. However, with each change of cycle of the supercapacitors charge and discharge, very fast over voltages appear (transient effects). This last is due to the fact that: when the supercapacitors are charged, the battery provides the power to the 42 V

Power Net. The DC/DC converter between supercapacitors and the DC bus is controlled by current. When the current load changes, battery is disconnected and supercapacitors give the power requirement. This commutation causes perturbations to the controller, and DC bus voltage varies. However, this transient effect is very fast and has no influence in operating system.

6. Conclusion

In this paper, we have presented presents a 42 V Power Net for automotive electrical system applications. The considered process is composed by a battery and a pack of supercapacitors and is modelized using MATLAB/SIMULINK® software. Simulation and experimental results show that the supercapacitor model with one RC branch can describe the supercapacitor behaviour in power applications. A microcontroller realizes the control and the energy management of the system. Notice that, unless some simplifications (particularly the converters switches) in our analysis, simulation and experimental results seem to be good agreement.

In the future, we project to substitute the PI controller used in this study by some modern approaches as a Neural Network controller.

References

[1] J.P.H. Shu, The development of the hybrid propulsion system for the light-duty vehicle applications, in: International Electric Vehicle Symposium and Exposition, EVS-20: Powering Sustainable Transportation, Long Beach, California (USA), November 15–19, 2003.
[2] E.J. Dowgiallo, A.F. Burke, Ultracapacitors for electric and hybrid vehicles, in: Electric Vehicle Conference, Florence, Italy, 1993.
[3] J. Lott, Helmut Späth Double layer capacitors as additional power source in electric vehicles, in: 18th International Electric Vehicle Symposium and Exhibition, Berlin, Germany, 2001, CD ROM.
[4] T. Dietrich, UltraCaps—a new energy storage device for peak power applications, in: 18th International Electric Vehicle Symposium and Exhibition, Berlin, Germany, 2001, CD ROM.
[5] L. Bertoni, H. Gualous, D. Bouquain, D. Hissel, M.C. Péra, J.M. Kauffinann, Hybrid auxiliary power unit (APU) for automotive applications, in: Proceedings of the IEEE Vehicular Technology VTC'02 Conference, Vancouver, Canada, 2002, ISBN 0-7803-7468-1, CD-ROM.
[6] D. Kok, E. Spijker, A. Seibertz, S. Buller, 42 V energy storage systems for stop–start application in hybrid vehicles, in: The 18th International Electric Vehicle Symposium and Exhibition, Berlin, Germany, 2001.
[7] Jin-uk Jeong, Hyeoun-dong Lee, Chul-soo Kim, Hang-Seok Choi, Bo H. Cho, A development of an energy storage system for hybrid electric vehicles using supercapacitor, in: The 19th International Battery, Hybrid and Fuel Cell Electric Vehicle Symposium and Exhibition, (EVS 19) BEXCO, Busan, Korea, 2002, pp. 1379–1389.
[8] R. Kötz, M. Carlen, Principles and applications of electrochemical capacitors, Electrochim. Acta 45 (2000) 2483–2498.
[9] A. Braun, M. Bärtsch, O. Merlo, B. Schnyder, B. Schaffiier, R. Kötz, O. Haas, A. Wokaum, Exponential growth of electrochemical double layer capacitance in glassy carbon during thermal oxidation, Carbon 41 (2003) 759–765.
[10] A. Matsuda, H. Honjo, M. Tatsumisaga, T. Minami, Electric double-layer capacitors using $HClO_4$-doped silica gels as a solid electrolyte, Solid State Ionics 113–115 (1998) 97–102.
[11] A. Yoshida, An electric double-layer capacitor with high capacitance and low resistance, IEEE Trans. Components Hybrids Manuf. Technol. 15 (l) (1992) 133–138.
[12] G.L. Bullard, H.B. Sierra-Alcazar, H.L. Lee, J.L. Morris, Operating principles of the ultracapacitor, IEEE Trans. Magnetics 25 (January (1)) (1989).
[13] B.E. Conway, Electrochemical Supercapacitors, Kluwer Academic Publishers/Plenum Press, New York, 1999, pp. 335–452.
[14] D. Qu, H. Shi, Studies of activated carbons used in double-layer capacitors, J. Power Sources 74 (1998) 99–107.
[15] A. Burke, Ultracapacitor: why, how, and where is the technology, J. Power Sources 91 (2000) 37–50.
[16] M. Hann, M. Baertschi, O. Barbieri, J.-C. Sauter, R. Kötz, GallayF R., Interfacial capacitance and electronic conductance of activated carbon double layer electrodes, Electrochem. Solid State Lett. 7 (2) (2004) A33–A36.
[17] M. Yoshimura, K. Honda, R. Uchikado, T. Kondo, T.N. Rao, Electrochemical characterization of nanoporous honeycomb diamond electrodes in non-aqueous electrolytes, Diamond Relat. Mater. 10 (2001) 620–626.
[18] E. Karden, S. Buller, R.W. De Doncker, A frequency-domain approach to dynamical modeling of electrochemical power sources, Electrochim. Acta 47 (2002) 2347–2356.
[19] L. Zubieta, R. Bonert, Characterization of double-layer capacitors for power electronics applications, IEEE-IAS'98 (1998) 1149–1154.
[20] L. Zubieta, R. Bonert, Characterization of double-layer capacitors for power electronics applications, IEEE Trans. Ind. Appl. 36 (January–February (1)) (2000) 199–205.
[21] H. Gualous, D. Bouquain, A. Bertbon, J.M. Kauffinann, Experimental study of supercapacitor serial resistance and capacitance variations with temperature, J. Power Sources 123 (2003) 86–93.
[22] J.-Y. Choi, B.H. Cho, H.F. VanLandingham, H.-s. Mok, J.-H. Song, System identification of power converters based on a black-box approach, IEEE Transactions on circuits and systems-I: Fundamental Theory and Applications 45 (11) (November 1998) 1148–1158.
[23] A. Djerdir, H. Gualous, D. Bouquain, A. Berthon, M.Y. Ayad, I. Rasoanarivo, S. Raël, B. Davat, Utilisation de supercondensateurs dans la motorisation de véhicules électriques à pile à combustible, in: Piles à Combustible et Interfaces pour les transports, Belfort, November, 2000.
[24] J. Syder, T. Heeg, A. O'Dwyer, Dead time compensators: performance and robustness issues, in: Proceedings of Process Control and Instrumentation 2000 Conference, Glasgow, Scotland, July 2000.
[25] D. Vrancic, S. Strmcnik, Practical guidelines for tuning PID controllers by using MOMI method, in: Proceedings of the IEEE International Symposium on Industrial Electronics, vol. 3, July 12–16, Bled, 1999, pp. 1130–1134.
[26] B. Choi, J. Kim, B.H. Cho, S. Choi, C.M. Wildrick, Designing control loop for DC-to-DC converters loaded with unknown AC dynamics, IEEE Transactions on Industrial Electronics 49 (4) (August 2002) 925–932.
[27] J. Herminjard, C. Zimmermann, R. Monnier, Three-phase unity power factor AC/DC converter with dual isolated DC/DC converter for a battery charger, EPE 99: European Conference on Power Electronics and Applications, Lausanne, Switzerland, September 1999. CD-ROM.
[28] M. Michael, D. Ross, A simple comprehensive lead-acid battery model for hybrid system simulation, CANMET Energy Technology Centre Varennes, CETC number 20002-049 (OP-J), September 2002.